Pseudo-biased coherent diffusion for robust real-time ultrasound speckle reduction

Khaled Z. Abd-Elmoniem, Abou-Bakr M. Youssef, and Yasser M. Kadah

Biomedical Engineering Department, Cairo University, Giza 12211, Egypt

ABSTRACT

We propose a novel technique for ultrasound speckle reduction based on iterative solutions to the coherent diffusion equation with the speckled image considered as the initial heat distribution. According to the extent of speckle, the model changes progressively from isotropic diffusion through anisotropic coherent diffusion to mean curvature motion. This structure maximally low-pass filters those parts of the image corresponding to fully-formed speckle, while preserving information associated with resolved object structures. The distance measure used to assess the deviation between images is embedded within the diffusivity tensor and is utilized as an intrinsic stopping criterion that ends the diffusion process completely in all directions when the deviation between the original and the filtered image exceeds the speckle limit. This model is termed pseudo-biased diffusion due to this unique formulation. Hence, there is no need for specifying the number of iterations in advance as with previous methods. Moreover, the steady state solution does not converge to the trivial single gray level solution, but rather to an image that is close in structure to the original but with speckle noise substantially reduced. Efficient discretization schemes allow large time steps to be used in obtaining the solution to achieve real-time processing.

Keywords: nonlinear coherent diffusion, speckle reduction, denoising.

1. INTRODUCTION

Ultrasound B-scan echo imaging involves signals obtained by coherent summation of echo signals from ultrasound scatterers located in the tissue under investigation. These scatterers arise from inhomogeneities and structures of sizes smaller than the wavelengths of ultrasound incident wave that are not resolved by the imaging system. The coherent summation of signals gives rise to an interference pattern commonly known as speckle. This speckle has a random nature since it is formed by signals from randomly located scatterers. The analysis of this speckle has been a major subject of investigation as it can be seen as unwanted nuisance because it may obscure structures in medium under observation. Alternatively, in other situations, it can be seen as a signal that is carrying important information on underlying randomly distributed scatterers. Therefore, the analysis of the echo envelope took two diverging directions to address the problems of speckle removal and characterization of speckle pattern to classify media [2,3,5,6].

1.1. Background

It has been shown that under the condition of large number of randomly located scatterers with small scatter spacing compared to wavelength of ultrasound, the statistics of the envelope signal show a Rayleigh distribution [4,7,11]. In such scattering regime, the only information available about the signal is the mean backscattered power. The interference pattern in the echo images under such regime is known as fully formed speckle (FFS). Raleigh statistical model requires scatterer densities of ten scatterers or higher per resolution cell. In practical situations, other patterns occur where there is a coherent component (structural nonrandom component that are larger than a wavelength) present in the echo signal or when the effective scatterer density is below ten which is the lower limit of Rayleigh model. Deviations from Raleigh distributed speckle pattern in such special scattering conditions have been previously modeled via Rice distribution to account for the addition of structural or non-random coherent component to the backscattered signal. In addition, the K distribution has been used to account for deviations to non-uniformity in scatterer distribution and for reduced scatterer densities [5,7,10].

Clinical ultrasound imaging systems employ nonlinear amplification to reduce the dynamic range of the input echo signal to match the small dynamic range of common display devices. The input signal usually has a dynamic range in the order of 70-100 dB whereas a typical display would have a dynamic range in the order of 20-30 dB. Such reduction is conventionally achieved using logarithmic amplification. This nonlinear amplification totally changes the statistics of the input envelope signal such that the evaluation of the modified statistics becomes difficult (detailed analysis on this subject

Medical Imaging 2001: Image Processing, Milan Sonka, Kenneth M. Hanson, Editors,
Proceedings of SPIE Vol. 4322 (2001) © 2001 SPIE · 1605-7422/01/$15.00

can be found in [9,10]). Due to the problem complexity, non-parametric methods for speckle reduction have gained wide acceptance in this field.

1.2. Current Methods for Speckle Reduction

Speckle degrades both spatial resolution and contrast in ultrasound images and thereby reduces the diagnostic value of the images. The aim of speckle reduction is to remove the distracting speckle pattern without affecting the diagnostic details in the ultrasound image, thus making ultrasound images easier to interpret. The problem of speckle reduction has been investigated extensively in the last two decades. Reduction was achieved using several methods. In maximum amplitude writing, several scans with different parameters are produced, the final image is formed from points of maximal amplitude at each spatial location. Speckle can also be reduced by forming an image from incoherent averaging of images with different speckle patterns. Such images may be acquired by varying the angle from which a target is imaged (a technique known as spatial compounding), or by changing the spectrum of acoustical pulse (frequency compounding) [1].

A more elaborate technique for such an application is nonlinear adaptive filtering. This filtering procedure recognizes those parts of an image that require maximal smoothing (i.e., which correspond to FFS). A measure of similarity has been used to maximally smooth regions of the image that closely resemble FFS. On the other hand, regions with properties that are least similar to FFS are not smoothed. Due to the simplicity of these models, blurring could not be avoided.

More advanced techniques for speckle reduction are based on the wavelet transform. Wavelet transform decomposes a signal (or an image) into Several increasingly smoother (also called low-pass filtered) scales. At each scale, the gradient or the Laplacian is estimated in each direction as an estimate of the high frequency components. The results are called wavelets and can be seen as band-pass filtered instances of the corresponding scale. Wavelet-based techniques remove wavelet coefficients at fine scales containing uncorrelated coefficients [16,18] or apply soft thresholding of wavelet coefficients in the Fourier domain to remove those coefficients with absolute values below a certain threshold [16,17]. Given that ultrasound images are characterized by a lower signal-to-noise ratio (SNR) than other imaging types, the wavelet-based techniques could not efficiently remove speckle in this type without severely distorting the image.

1.3. Overview

Generally speaking, an efficient speckle reduction algorithm must suppress FFS while substantially preserving the image component corresponding to resolved (or partially resolved) object structure. Our approach for reducing speckle is based on the theory of nonlinear coherent diffusion model [15,19]. Nevertheless, the evolution of the algorithm is controlled via a distance measure that is used to avoid large deviations between the original speckled image and the filtered one. In this paper, we review the nonlinear coherent diffusion model and present the biased diffusion model. Then, we derive a model that combines the attributes of both biased and coherent diffusion while taking advantage of the fast discretization scheme of [19]. The results of applying this algorithm to typical ultrasound images are presented. Finally, we discuss the applications of the new technique and provide ideas for future work.

2. METHODOLOGY

2.1. Approximate Speckle Noise Model

A general model for ultrasound images with speckle noise is,

$$f(x,y) = g(x,y)\eta_m(x,y) + \eta_a(x,y) \quad (1)$$

where $g(x,y)$ is an unknown piecewise constant 2-D function representing noise-free original image to be recovered, $f(x,y)$ is the noisy observation of $g(x,y)$, η_m and η_a are multiplicative and additive noise models respectively, and x and y are variables of spatial locations that belong to 2-D space of all real numbers $(x,y) \in \Re^2$. Since the effect of additive noise (such as sensor noise) is considerably small compared to that of multiplicative noise (coherent interfering), $\left(\|\eta_a(x,y)\|^2 << \|\eta_m(x,y)\|^2\right)$, Eq. (1) can be approximated by,

$$f(x,y) = g(x,y)\eta_m(x,y) \quad (2)$$

The logarithmic amplification transforms the model in Eq. (2) into an additive one. That is,

$$\log\left(f(x,y)\right)=\log\left(g(x,y)\right)+\log\left(\eta_m(x,y)\right), \tag{3}$$

or

$$f^l(x,y)=g^l(x,y)+\eta_a^l(x,y), \tag{4}$$

where $\eta_a^l(x,y)$ is approximated as additive white noise [8,12].

2.2. Original Nonlinear Diffusion Formulation

Consider an m-dimensional rectangular image domain $\Omega=(0,a_1)\times\cdots\times(0,a_m)$ with boundary $\partial\Omega$, and a gray level image given by a bounded mapping $f:\Omega\to\Re$. In scale-space theory, an image is embedded into a continuous family $\{T_t f \mid t\geq 0\}$ of gradually smoother (diffused) versions of it. The original image corresponds to scale $t = 0$ and increasing the scale should simplify the image without creating spurious structures. Nonlinear anisotropic diffusion was first proposed to avoid the blurring and localization problems of linear filtering. That is, to further encourage smoothing within a region in preference to smoothing across the boundaries [13]. This non-uniform process reduces the diffusivity at those locations that have a larger likelihood to be edges since they reveal larger gradients. Perona and Malik obtained the filtered image $I(x,t)$ as a solution of the nonlinear diffusion equation with the original image as initial condition and reflecting boundary conditions (μ_1 denotes the derivative normal to the image boundary $\partial\Omega$):

$$\partial_t I = div\left(g\left(|\nabla I|^2\right)\nabla I\right) \quad on \quad \Omega\times(0,\infty), \tag{5}$$

$$I(x,0) = f(x) \quad on \quad \Omega, \tag{6}$$

$$\partial_n I = 0 \quad on \quad \partial\Omega\times(0,\infty). \tag{7}$$

Eq. (7) is the mathematical formulation of the reflecting boundary conditions, which are also called *Neumann* boundary conditions. The time t is a smoothing parameter; larger values correspond to simpler (or blurred) image representations $I(x,t)$. $g\left(|\nabla I|^2\right)$ is a monotonically decreasing diffusivity that takes the form:

$$g(s)=\frac{1}{1+s/\lambda^2}\ ,(\lambda>0) \qquad \text{or} \qquad g(s)=1-exp\left(-\frac{1}{(s/\lambda)^{2n}}\right)\ ,(\lambda>0)$$

In general, $g(x)$ can be expressed in a tensor form that measures local coherence of structures. In such cases, the anisotropy of the diffusion process becomes more directional in both the gradient and the contour directions, the directions of maximum and minimum variations respectively.

2.3. Biased Nonlinear Diffusion

The evolution of Eq. (5) converges to an equilibrium state at which:

$$\Delta^2 I(t_\infty)=0, \tag{8}$$

which occurs only when the intensity map reaches a single flat value. Due to this uninhibited single gray level equilibrium solution of the nonlinear diffusion equation, an additional term was proposed to make the steady state solution a nontrivial one [14]. In this case, the modified diffusion equation takes the form,

$$\partial_t I = div\left(g\left(|\nabla I|^2\right)\nabla I\right)+\left(I(t_0)-I(t)\right). \tag{9}$$

This formulation converges to a steady state value at which,

$$\Delta^2 I(t_\infty)\approx I(t_0)-I(t_\infty). \tag{10}$$

With the formulation of Eq. (9), the images are repeatedly filtered until a nontrivial steady state is reached without need to specify the number of iterations. Nevertheless, this bias term $(I(t_0)-I(t))$ is responsible for increasing the complexity of the differential equation such that only the forward discretization scheme can be used for the numerical solution. In practical situations, the equilibrium state in Eq. (10) needs an evolution time of more than five or six. With forward discretization scheme, the evolution of the differential equation is limited to a time step $\Delta t \le 1/(2m)$, where m is the number of dimensions, to maintain the stability of this method. This translates into a large number of iterations of more than 24 on 2D images, which makes the processing time of the technique prohibitively slow.

2.4. Coherent Nonlinear Anisotropic Diffusion

The coherent diffusion model takes the form,

$$\partial \boldsymbol{I}(x,y,t)/\partial t = div[D\nabla \boldsymbol{I}], \tag{11}$$

where $D \in \Re^{2\times 2}$ is a symmetric positive semi-definite diffusion tensor representing the required diffusion in both gradient and contour directions and hence enhancing coherent structures as well as edges. There are two tensors widely used to detect the local coherence: the structure tensor (also called scatter matrix or windowed second moment tensor), and the Hessian tensor which represents the second order derivatives.

$$\underbrace{\begin{pmatrix} I_x{}^2 & I_x I_y \\ I_x I_y & I_y{}^2 \end{pmatrix}}_{\text{Structure matrix}} \qquad \underbrace{\begin{pmatrix} I_{xx} & I_{xy} \\ I_{xy} & I_{yy} \end{pmatrix}}_{\text{Covariance (Hessian) matrix}} .$$

Because the Hessian matrix was found more sensitive to noise, the structure tensor form will be used throughout this paper. The multi-scale (or window) structure matrix takes the form

$$\begin{aligned} J_\rho(\nabla I) &= K_\rho * (\nabla I \otimes \nabla I) \\ &= K_\rho * \left(\nabla I \cdot \nabla I^T\right) \qquad (\rho \ge 0) \end{aligned}$$

Or equivalently,

$$J_\rho(I) = \begin{pmatrix} K_\rho * I_x^2 & K_\rho * (I_x I_y) \\ K_\rho * (I_x I_y) & K_\rho * I_y^2 \end{pmatrix}, \tag{12}$$

where,

$$K_\sigma(x) = \left(2\pi\sigma^2\right)^{-1} \cdot \exp\left(|x|^2 / 2\sigma^2\right).$$

The convolution above is done component-wise mainly to average a feature over a known neighborhood (scale) where ρ is the integration scale (or window size) over which the orientation information is averaged [15].

The formulation in Eq. (12) can be put as,

$$J(I) = \begin{pmatrix} w_1 & w_2 \end{pmatrix} \begin{pmatrix} \mu_1 & 0 \\ 0 & \mu_2 \end{pmatrix} \begin{pmatrix} w_1^T \\ w_2^T \end{pmatrix}. \tag{13}$$

The eigenvectors w_1, w_2 and the eigenvalues μ_1, μ_2 correspond to the directions of maximum and minimum variations and the strength of these variations respectively.

2.5. Coherent Diffusion for Speckle Reduction

The diffusion tensor D should be chosen with the same eigenvectors of the structure matrix but with adaptive eigenvalues that represent the strength of diffusion in each principal direction. In particular, we use the following specifications for the diffusion tensor [19],

$$D(I) = \begin{pmatrix} w_1 & w_2 \end{pmatrix} \begin{pmatrix} \lambda_1 & 0 \\ 0 & \lambda_2 \end{pmatrix} \begin{pmatrix} w_1^T \\ w_2^T \end{pmatrix},$$

where,

$$\lambda_1 = \begin{cases} \alpha \cdot \left(1 - (\mu_1 - \mu_2)^2 / s^2\right) & , if\ (\mu_1 - \mu_2)^2 / s^2 \le 1 \\ 0 & , otherwise \end{cases}$$
$$\lambda_2 = \alpha \qquad , everywhere \tag{14}$$

The analysis of this model will be fully described within the framework of the proposed pseudo-biased diffusion in the next section.

3. PSEUDO-BIASED DIFFUSION

Although the previous model has proved to be efficient in removing speckle, however, without prior knowledge of the appropriate time evolution needed to reach this speckle free image, the model continues to evolve to the trivial solution. This behavior is not recommended for parameter robustness. The overall time step is a very important parameter that drastically influences the final status of the filtered image. However, the behavior of a robust filtering algorithm should not be sensitive to parameter selection especially to the time evolution. Therefore, the flow dynamics of the diffusion process should be controlled based on both the spatial local coherence and also the temporal distance between the original speckled image and the current evolved image. Meanwhile, the added diffusion control should not increase (at least, minimally) the complexity of the numerical implementation of the process.

3.1. Proposed Model Formulation

The proposed model can be summarized in the design for the required diffusion eigenvalues:

Let,

$$\delta = 1 - \beta \cdot \left(\left|I(t_0) - I(t)\right|\right) \ , \ 0 \le \beta \le 1 , \tag{15}$$

and,

$$\lambda_1 = \begin{cases} \alpha \cdot \delta \cdot \left(1 - (\mu_1 - \mu_2)^2 / s^2\right) & if\ (\mu_1 - \mu_2)^2 \le s^2 \\ 0 & else \end{cases}$$
$$\lambda_2 = \alpha \cdot \delta \tag{16}$$

The distance between the original and the evolved images (represented as in Eq. (15)) is continuously measured at all time instants and is embedded within the formulation of the eigenvalues to control the status of diffusion process. This modification has the effect of completely stopping the flow of the diffusion at any time and location where the deviation between the two images becomes unreasonable as will be analyzed.

3.2. Model Analysis

The dynamics of the proposed model can be clearly understood from the eigen-analysis framework. The flow is affected by two factors; the first one is the distance between the evolved image at any time t and the original image at time $t = 0$ (that we call *temporal distance*). The second factor is the spatial local coherence or anisotropy (*spatial coherence*).

At low time instants ($t \approx t_0$), the temporal distance effect is completely negligible ($\delta \approx 1$) and the only dominant factor is that of the spatial coherence. When the local coherence, measured by $(\mu_1 - \mu_2)$, is close to zero, i.e., the region corresponds to speckle pattern close to FFS carrying little tissue information, diffusion must become isotropic ($\mu_1 \approx \mu_2 = \alpha$) and inversely proportional to the information content (which is also related to $(\mu_1 - \mu_2)$). On the other hand, when image anisotropy becomes large, which corresponds to structured tissue, image texture is rich of information about the imaged tissue and therefore diffusion should be very selective in both direction and strength. This idea is implemented by the above mentioned Tukey's function, which is monotonically decreasing such that as information content increases, diffusion becomes more and more anisotropic. A fully structured region corresponding to $(\lambda_1 - \lambda_2)^2 > s^2$ is associated with diffusion only in contour direction.

As time evolution goes forward, the image continues to diffuse and some structures may be inevitably unsharpened. In such cases, the temporal distance increases between the original and diffused edge sharpness. The embedding of this distance in the diffusion matrix has the effect of choking extra diffusion in these locations. This effect dominates over the

effect of spatial coherence and thus, limiting diffusion. With time, the unshaped edges become relatively sharper than before with respect to inter-region fluctuations.

3.3. Discretization Scheme

The tensor-form nonlinear heat equation can be represented as:

$$\frac{\partial I}{\partial t} = div\left[\underbrace{\begin{pmatrix} a & b \\ c & d \end{pmatrix}}_{(diffusion\ matrix\ D)} \underbrace{\begin{pmatrix} I_x \\ I_y \end{pmatrix}}_{(gradient\ vector)}\right] \tag{17}$$

The corresponding difference equation involves all the 8-neighborhood points and thus can not be split by the traditional methods. The following discretization scheme was proposed:

$$I_{i,j}^{t+\Delta t} \Leftarrow \begin{pmatrix} I_{i-1,j+1}^{t} & I_{i,j+1}^{t+\Delta t} & I_{i+1,j+1}^{t} \\ I_{i-1,j}^{t+\Delta t} & I_{i,j}^{t} & I_{i+1,j}^{t+\Delta t} \\ I_{i-1,j-1}^{t} & I_{i,j-1}^{t+\Delta t} & I_{i+1,j-1}^{t} \end{pmatrix} \tag{18}$$

In this scheme, additive or multiplicative splitting can be used to convert the system matrix into two tridiagonal matrices that are easily solved [19].

4. RESULTS AND DISCUSSION

The model was first applied on images of a commercial contrast detail phantom (ATS laboratories, Bridgeport, CT) [10]. Contrast regions had varying scatterer number density to produce standard contrast levels from –15 dB to +12 dB. These images were logarithmically compressed in the post-processing stage to simulate compressed B-scan images. The phantom image size is 256x128 containing eight regions of different contrast values: four positive contrast regions and four negative contrast regions. Regions are ordered in two rows. The upper row contains the negative contrast regions while the lower contains the positive contrast regions. A reference image is constructed manually from the speckled image by evaluating the mean value in each region. The obtained results are compared with this reference image.

The model in Eq. (11) was applied with eigenvalues as in Eq. (14) to represent the unbiased diffusion and with eigenvalues of Eq. (16) to represent the proposed pseudo-biased diffusion. Both models utilized the same values for the common algorithm parameters. To clarify flow improvement by the proposed model, we did the phantom experiment with relaxed parameters. Both models were applied for 20 iterations with a time step $\Delta t = 3$ per iteration, $\alpha = 1$, $s = 70$, and $\beta = 0.05$ in the pseudo-biased model. Figure 1 shows the evolution of both models with successive iterations. Figure 4-(a, b) show the evolution of a line passing through different positive contrast regions with both models.

In the second experiment, the two algorithms were applied on a real gray scale ultrasound images. The first one shows a blood vessel and the second one shows the heart chambers, the size of both images is 256x256. In this experiment, we employed parameter values that are more conservative. Both models share the same parameters for 10 iterations with a time step $\Delta t = 2$ per iteration, $\alpha = 1$, $s = 20$, and $\beta = 0.2$ in the pseudo-biased model. Figure 2 and Figure 3 show the results obtained from the two images. Figure 4-(c, d) and (e, f) present the evolution of two lines through the images. Line positions in the original images are shown in reverse video in Figure 2-(g) and Figure 3-(g), respectively.

Edges of both phantom and vessel images have been restored better than with the pseudo-biased model even with excessive iterations. The unbiased model is still iteration-dependant and thus continues toward the trivial single gray level solution. Edge preservation and iteration-robustness of the proposed model come with minimal extra complexity in the implementation of the model. Both unbiased and pseudo-biased models take almost the same time per iteration.

Since the modification was merely in the determination of the diffusion components, the proposed model shares the unbiased diffusion the same simplicity of discretization. Only two additions and two multiplication operations are needed per pixel for embedding the distance component of Eq. (15). Considering the overall complexity, these additional operations are truly insignificant.

5. CONCLUSIONS

We presented in this paper a model for speckle reduction based on the nonlinear coherent diffusion that preserves coherent structures. Diffusion processes do not stop naturally unless it reaches to a non-varying single gray level image. Some authors preferred to use a biasing term to force the process to stop at a point other than the trivial solution. However, that model add extra complexity to the numerical iterative solution of the difference equation which make it unpractical with real data which need a large time of diffusion to smooth noise. The proposed model however, combines the advantages of simple discretization scheme presented in a previous paper and in the same time it has an imbedded (intrinsic) measure that stops diffusion naturally after a certain time and thus no need for specifying the number of iterations in advance. We are now involved in the analysis of the effect of other parameters of the model and the sensitivity to each of them trying to find a certain measure for automatic selection of these parameters.

ACKNOWLEDGEMENTS

This research is supported in part from the R&D Department at International Electronics, Biomedical Division, 6 October City, Egypt.

REFERENCES

1. G. Trahey et al., "A Quantitative Approach to Speckle Reduction via Frequency Compounding," *Ultrasonic Imaging*, **8**, pp. 151-164, July 1986.
2. J. Bamber and C. Daft, "Adaptive Filtering For Reduction of Speckle in Ultrasonic pulse-echo Images," *Ultrasonics*, **24**, pp. 41-44, Jan. 1986.
3. J. C. Bamber and J. V. Philps, "Real-time implementation of coherent speckle suppression in B-scan images," *Ultrasonics*, **29**, pp. 218-224, May 1991.
4. C. B. Burkhardt, "Speckle in Ultrasound B-Mode Scans," *IEEE Trans. Son. Ultrason.*, **SU-25**, no. 1, pp. 1-6, Jan. 1978.
5. R. F. Wagner and M. F. Insana, "Analysis of ultrasound image texture via generalized Rician statistics," *Proc. SPIE* **556**, pp. 153-159,1985.
6. R. F. Wagner, M. F. Insana, and D. G. Brown, "Unified approach to the detection and classification of speckle texture in diagnostic ultrasound," *Opt. Eng.*, **25**, pp. 738-742, June 1986.
7. T. A. Tuthill, R. H. Sperry, and K. J. Parker, "Deviation from Rayleigh statistics in ultrasonic speckle," *Ultrasound Imaging*, **10**, pp. 81-90, April 1988.
8. A. K. Jain, *Fundamentals of Digital Image Processing*. Englewood Cliffs, NJ: Prentice-Hall, 1989.
9. D. C. Crowford, D. S. Bell, and J. C. Bamber, "Compensation for the signal processing characteristics of ultrasound B-mode scanners in adaptive speckle reduction," *Ultrasound in Med. & Biol.*, **19**, pp. 469-485, 1993.
10. Vinayak Dutt, "Statistical analysis of ultrasound echo-envelope", *Ph.D. thesis*, Mayo Graduate School, 1995.
11. J. W. Goodman, "Some fundamental properties of speckle," *J. Opt. Soc. Amer.*, **66**, no. 11, pp. 1145-1150,1976.
12. X. Zong, A. F. Laine, and E. A. Geiser, "Speckle Reduction and Contrast Enhancement of Echocardiograms via Multiscale Nonlinear Processing," *IEEE Trans. Med. Img.*, **17**, no. 4, Aug. 1998.
13. P. Perona and J. Malik, "Scale space and edge detection using anisotropic diffusion," *IEEE Trans. PAMI*, **12**, no. 7, pp. 629-639, July 1990.
14. N. Nordstrom, "Biased anisotropic diffusion –A unified regularization and diffusion approach to edge detection," *Image Vision Comput.*, **8**, no. 4, pp. 318-327, 1990.
15. J. Weickert, "Multiscale texture enhancement," *Computer analysis of images and patterns, Lecture notes in. Comp. Science*, **970**, Berlin, pp. 230-237,1995.
16. Akram Aldroubi and Michael Unser, *Wavelets in Medicine and Biology*, New York: CRC Press, 1996.
17. Xuli Zong, et al., "Speckle Reduction and Contrast Enhancement of Echocardiograms via Multiscale Nonlinear Processing," *IEEE Trans. Med. Imaging*, **17**, no. 4, pp. 532-540, August 1998.
18. Yansun Xu, et al., "Wavelet Transform Domain Filters: A Spatially Selective Noise Filtration Technique," *IEEE Trans. Img. Proc.*, **3**, no. 6, pp. 747-758, Nov. 1994.
19. Khaled Z. Abd-Elmoniem, Yasser M. Kadah, Abou-Bakr M. Youssef, "Real Time Adaptive Ultrasound Speckle Reduction and Coherence Enhancement," *Int. Conf. of Image Processing, ICIP' 2000.*

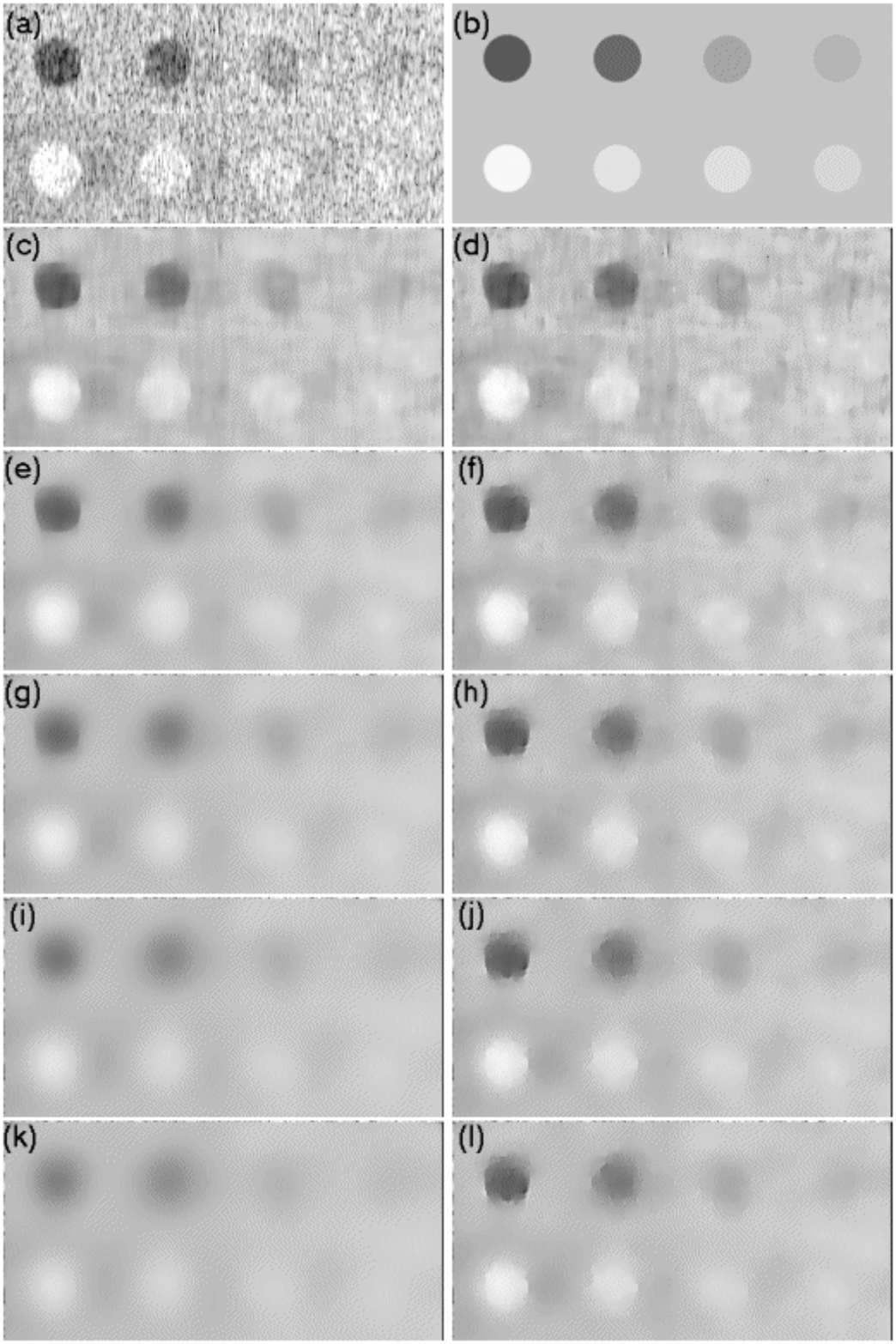

Figure 1: Phantom results. (a) Speckled image. (b) Reference image. (c, e, g, i, k) Evolution of unbiased diffusion after 4, 8, 12, 16, and 20 iterations respectively. (d, f, h, j, l) Evolution of pseudo-biased diffusion after 4, 8, 12, 16, and 20 iterations respectively.

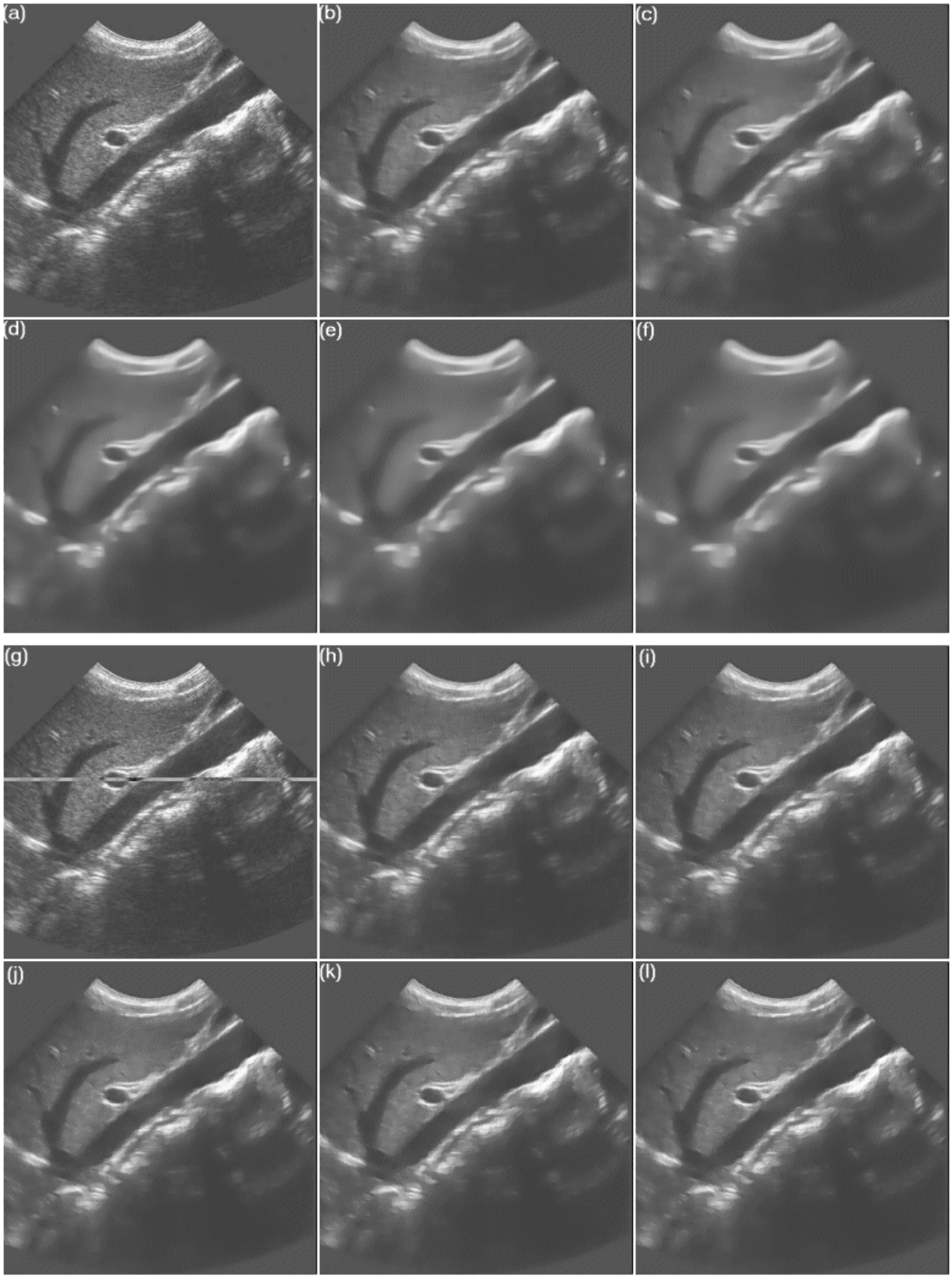

Figure 2: The evolution of a real ultrasound image with both models. (a) Original speckled image. (b, c, d, e, f) The evolution with the unbiased diffusion after 2, 4, 6, 8, 10 iterations respectively. (g) Speckled image with a detail line position indicated. (h, i, j, k, l) present the evolution with the pseudo-biased model after 2, 4, 6, 8, 10 iterations respectively.

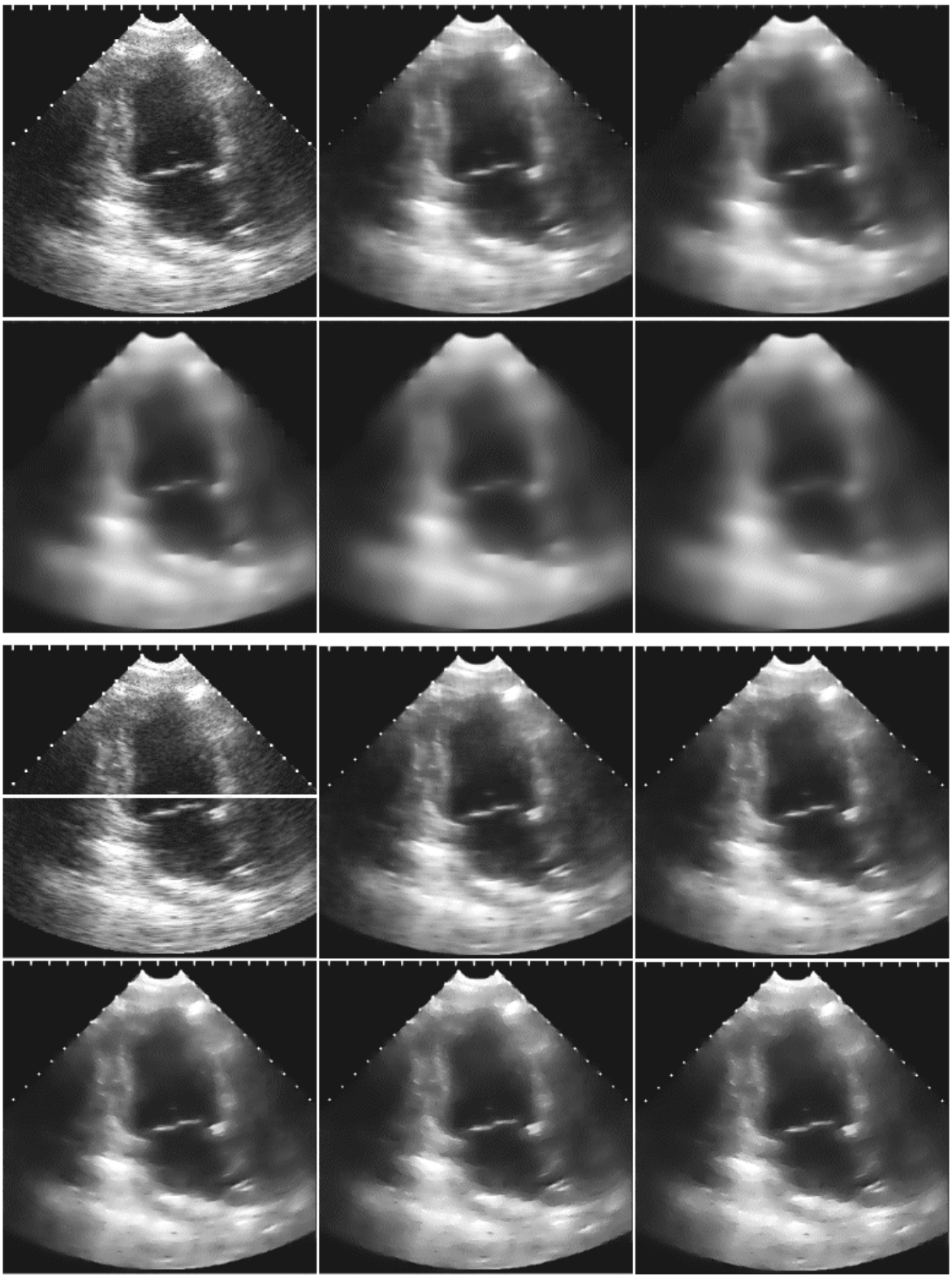

Figure 3: The evolution of a real ultrasound image of the heart with both models. (a) Original speckled image. (b, c, d, e, f) The evolution with the unbiased diffusion after 2, 4, 6, 8, 10 iterations respectively. (g) Speckled image with a detail line position indicated. (h, i, j, k, l) present the evolution with the pseudo-biased model after 2, 4, 6, 8, 10 iterations respectively.

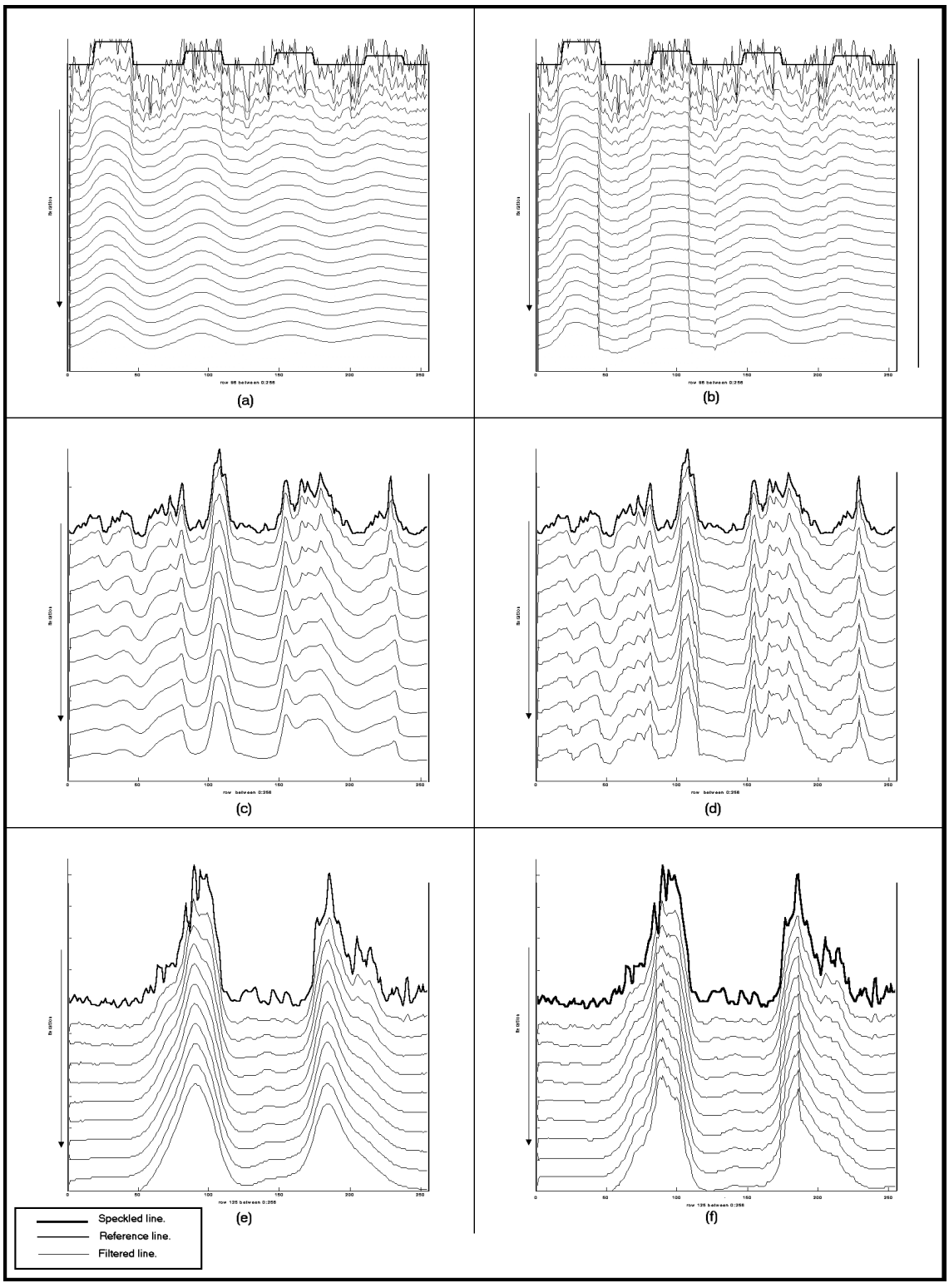

Figure 4: Plotting of line from images of previous figures exploring the evolution with unbiased diffusion (Left). The evolution with pseudo-biased diffusion (right). Up: A positive contrast line from Figure 1. Middle: A line whose position is marked in Figure 2-g. Down: A line whose position is marked in Figure 3-g.